Optimization of X-Ray Sources from a High-Average-Power Nd:Glass Laser-Produced Plasma for Proximity Lithography

P. Celliers *S. Mrowka* *D. Matthews*

L. B. Da Silva *M. Norton* *J. A. Abate**

C. B. Dane *L. Hackel* *J. Maldonado*†

Introduction

The concept of a laser-based proximity lithography system for electronic microcircuit production has advanced to the point where a detailed design of a prototype system capable of exposing wafers at 40 wafer levels per hr is technically feasible with high-average-power laser technology. In proximity x-ray lithography, a photoresist composed of polymethylmethacrylate (PMMA) or similar material is exposed to x rays transmitted through a mask placed near the photoresist, a procedure which is similar to making a photographic contact print. The mask contains a pattern of opaque metal features, with line widths as small as 0.12 μm, placed on a thin (1-μm thick) Si membrane. During the exposure, the shadow of the mask projected onto the resist produces in the physical and chemical properties of the resist a pattern of variation with the same size and shape as the features contained in the metal mask. This pattern can be further processed to produce microscopic structures in the Si substrate.

The main application envisioned for this technology is the production of electronic microcircuits with spatial features significantly smaller than currently achievable with conventional optical lithographic techniques (0.12 μm vs 0.25 μm). This article describes work on optimizing a laser-produced plasma x-ray source intended for microcircuit production by proximity lithography.

Background

To obtain the best transmission through the Si substrate, followed by absorption in the PMMA, the illumination source should occupy a band of x-ray wavelengths somewhere above the Si K-edge (6.74 Å) but long enough that the x rays are efficiently absorbed in the PMMA resist layer (possibly up to 15 Å). The x-ray wavelength is short enough that blurring due to x-ray diffraction from edges in the pattern will not be significant. Current system designs for proximity lithography require a source with a median emission wavelength in the range of 10–14 Å and a 20% bandwidth. The mask can be illuminated with a collimated source of x rays, such as from a synchrotron tuned to operate at the desired wavelengths. In fact, the basic principles of proximity lithography have already been demonstrated using synchrotron sources.[1,2] However, synchrotron facilities are inherently expensive and therefore not amenable for most circuit manufacturers to acquire and operate.

Laser-produced plasmas have been recognized as a promising alternative to synchrotrons for a number of years. The physical specifications that the plasma source must meet can be summarized as follows: the source must deliver approximately 15 mJ/cm^2 of x-ray fluence to the resist with a uniformity of 1% over a 3×3 cm^2 area within an exposure interval of approximately 1.3 s; the x-ray spectrum must occupy a 20% bandwidth centered on a wavelength ~12 Å. These requirements can be met using a 1-kW laser assuming about $10\%/(2\pi$ sr) conversion of laser energy into the desired x-ray band; the mask and resist are assumed to be about 50 cm from the source point to satisfy the uniformity requirements. Variations on these figures may occur depending on a number of design options, but it is clear that in any system a substantial portion of the costs are directly

* AT&T Bell Laboratories, Murray Hill, New Jersey

† IBM Microelectronics, Hopewell Junction, New York

driven by the average power level needed from the laser, which in turn hinges on achieving high x-ray yields.

X-ray yields from laser-produced plasmas have been investigated in great detail for nearly two decades and have been examined over a wide variety of laser parameters (wavelength, pulse duration, focused intensity) as well as target material and x-ray emission wavelengths.[3–12] Several studies have focused specifically on lithography applications to match target materials with realistic laser parameters to produce the required x-ray spectrum (keV x rays) at an acceptable yield.[13–19] X rays from laser-produced plasmas in the 1-keV energy range required for proximity lithography are produced most efficiently with focused laser intensities around 10^{13} W/cm^2 and from targets with atomic numbers in the range Z = 26–30 (Ne-like ions, L-shell emission) or Z = 53–56 (Ni-like ions, M-shell emission). As a general finding, x-ray yields are known to improve substantially with decreasing laser wavelength.[4,5,7]

X-ray yields from laser-produced plasmas also depend on the pulse duration, which determines the characteristic plasma volume achieved during the pulse. High conversion efficiency has been usually observed with moderate-duration pulses (0.5–10 ns).[11,16] However, it can also be achieved with shorter pulses (<100 ps) in combination with a weak prepulse to generate a long-scale-length plasma.[12,20] It is not clear from the findings of previous studies whether high conversion efficiency can be achieved from pulses longer than 10 ns. Experiments with 8-ns Nd:glass laser pulses indicate that efficiencies around 8%/(2π sr) could be achieved.[3] However, experiments with 30-ns KrF pulses focused to more than 10^{14} W/cm^2 failed to achieve yields comparable to measurements with shorter pulses at the same wavelength.[17] Chaker et al.[19] suggest a practical limit on the pulse duration of less than about 5 ns, but this conclusion is tentative in the absence of experimental data. The requirements of high average power with high focused intensities and moderate pulse duration are potentially in conflict with the pulse parameters of current high-average-power laser technology, which operate more reliably with rather long pulse durations in the range of 10–15 ns for Nd:glass technology and 25–30 ns for excimer lasers.

One potential laser driver for proximity lithography is a high-average-power Nd:glass slab design operating with high pulse energy and moderate repetition rate. Currently, the most advanced realization of this technology is available at Lawrence Livermore National Laboratory (LLNL)[21] and consists of a flash-lamp-pumped system capable of producing near-diffraction-limited pulses with approximately 13-ns full-width at half maximum (FWHM) duration at energies of ~20 J at a rate of 6 Hz to produce an average power of 120 W. The design is scalable to higher average power by increasing the pulse energy and/or repetition rate; we envision average powers approaching 2 kW. An important characteristic of this high-average-power capability is the use of phase conjugate wavefront correction[22] to ensure a uniform intensity and a near ideal phase front in the final pass of the slab amplifier, which is necessary to ensure reliable operation. This technology operates most effectively with a rather long pulse duration (12–14 ns), which raises the issue of whether the x-ray yields produced with this laser can approach the maximum yields observed with shorter pulses. We examined this issue experimentally in the work described in this article.

Experiment

We measured and optimized the x-ray conversion efficiency from several L-shell emitters (Fe, Cu, Zn, brass, stainless steel) and one M-shell emitter (Xe). The studies with Xe examined the solid form using a cryogenic target. In addition to producing high x-ray yields at the desired wavelengths, Xe targets offer the potential to design a source with considerably reduced debris generation. We investigated all targets at two operating wavelengths of the laser: the fundamental wavelength, 1.053 μm, and the second harmonic, 0.527 μm.

Figure 1 shows the layout for the experiments with solid planar targets. This section describes the five main parts identified by Fig. 1: the laser beam, the solid targets, the charge-coupled device (CCD) camera and spectrometer system, the filtered photoconductive diamond (PCD) detectors, and the pinhole camera.

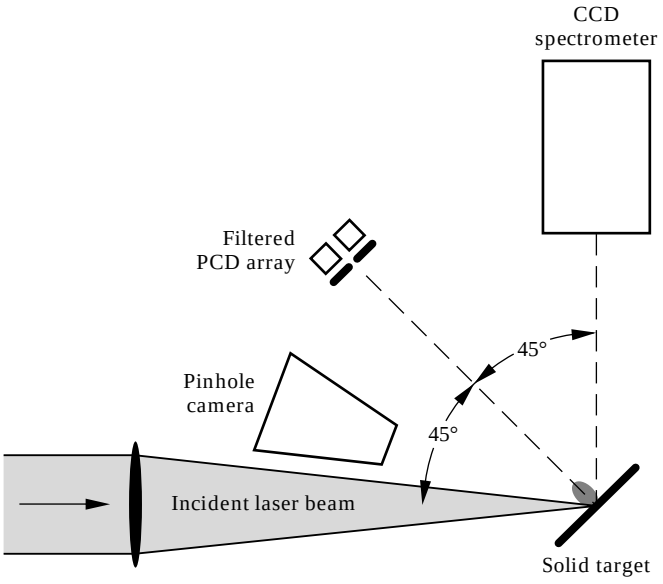

FIGURE 1. Experimental arrangement employed for solid target x-ray yield measurements. (10-06-0595-1100pb01)

Laser Parameters

A 330-mm lens focused the laser into the center of the experimental chamber onto a planar target oriented at 45° to the laser axis. We monitored the laser energy with a fast pyroelectric detector and cross-calibrated it with a calorimetric energy meter. Pulse energy varied from ~1–20 J at 1.053 μm and ~0.5–12 J at 0.527 μm. The beam delivered to the target chamber was square in cross-section, measuring 25 mm per side. We used a 330-mm focal-length lens to produce an $f/13$ focus. We adjusted the beam focus by translating the lens on a translation stage. In a separate test of the beam quality, we projected a series of far-field beam images with 0.527-μm light onto a CCD camera using a well corrected microscope objective. We found that, at best focus, 80% of the beam energy was contained within a diameter of 27 μm, equivalent to about 1.5× diffraction limit. The maximum focused intensities achieved with this beam quality are 7×10^{13} W/cm^2 for 1.053-μm light and 2×10^{14} W/cm^2 for 0.527-μm light. These peak intensities meet or exceed the intensities needed to obtain good x-ray yields in the kilovolt range.

Solid Targets

The target mount consisted of an x–y–z translation stage with an aluminum mounting frame for attaching the target. Motion in a plane parallel to the target surface (x–y) allowed us to position a fresh surface of the target in the beam for each shot while maintaining the same axial position relative to the laser focus. All of the solid targets could be mounted (as tapes or thin plates) directly onto the mounting frame. For most of these materials, the target thickness was much larger than typical ablation depths. In the particular case of Fe, however, the target consisted of a thin layer of Fe powder (3–5 μm) bonded to a mylar tape substrate. This "mass-limited" target is designed to provide enough material to produce x rays while limiting debris production.

In the particular case of solid Xe, the target apparatus consisted of a 1-mm-thick Cu plate thermally connected with a 2-in-long Cu braid to a cold finger and cooled to approximately 20 K. By condensing Xe gas onto the cryogenic surface, we produced a thin (~100 μm), solid Xe layer on the Cu substrate. Although the melting point of Xe (at atmospheric pressure) is around 160 K, a temperature of 20 K was required in vacuum to maintain a low enough Xe vapor pressure to produce a stable condensed layer on the Cu substrate and to minimize reabsorption of the Xe emission by residual cold Xe gas in the chamber.

Curved Crystal Spectrograph

To determine x-ray yields, we needed accurate measurements of the x-ray spectrum produced by each source. The spectra varied not only with target material, but also with the laser parameters (wavelength, pulse energy, and focus). A curved potassium acid pthalate (KAP) crystal spectrograph recorded x-ray spectra 90° relative to the laser axis and 45° to the target normal, using a high-resolution CCD camera system operating with 16-bit readout resolution.[23] The spectrometer—three separate KAP crystals bent to the same radius of 79 mm—rested ~350 mm from the plasma. The detector was a back-illuminated Tektronix TK1024 CCD chip. The system was sensitive enough that all spectra recorded in these experiments were produced by a single laser pulse. To obtain the complete spectrum, we placed the KAP crystals at slightly different standoff distances from the plasma to sample the 9–19-Å spectral region in three overlapping segments. To block out visible and UV portions of the spectrum, we placed one or two layers of a light-tight aluminized mylar film (5000 Å Al/1.5 μm mylar) at the entrance to the spectrograph. This film was subject to occasional damage from target debris; therefore, we checked and replaced it at appropriate intervals.

We calibrated the spectrometer dispersion by identifying known features of the Fe and Cu L-shell spectrum and applying a low-order polynomial mapping from detector position to a wavelength scale. Within the 9–19-Å band, the CCD array detector responds linearly to the x-ray fluence independent of wavelength. Corrections had to be applied to the raw data to account for the filter transmission and the KAP crystal reflectivity. The filter transmission was independently calibrated at an in-house facility to determine its transmission over the 9–19-Å wavelength band. Henke, et al. previously calibrated the KAP reflectivity.[24]

Absolutely Calibrated PCD and Yield Measurements

We recorded x-ray yields with a set of four filtered type IIA PCD detectors.[25] These were mounted in a compact 2×2 square array 15.9 cm from the target at an angle approximately normal to the target surface. For all measurements, the PCDs were biased with 600 V, and the signal was coupled through a capacitor into a 50-Ω cable connected to a high-speed digital oscilloscope for recording. These detectors have been used in previous x-ray yield experiments at LLNL,[26] and have been absolutely calibrated.[27] Within the 9–19-Å wavelength band observed in these measurements, the detectors have a flat wavelength response. For the bias conditions and spectral range used in the measurements, the sensitivity of these devices was nominally 7.5×10^{-4} A/W. We assumed an uncertainty of approximately 20% on this value, as reported in the original absolute calibration.

Figure 2 shows examples of a PCD signal trace and a trace of the laser pulse recorded on high-speed oscilloscopes. The x-ray pulses displayed the same temporal structure, if any, produced in the laser pulses. The FWHM pulse duration of the x-ray signals observed from solid targets was similar to, but somewhat shorter than, the laser pulse by an amount ~20–30%. Hence the x-ray pulses from solids were typically 10 ns FWHM, while the laser pulse was 12–14 ns FWHM.

We monitored contributions from various parts of the x-ray spectrum using a set of four different filters on the PCD detector array. The filter set was designed to sample the 8–20-Å band in three intervals: a 10.6-μm Al filter (8–12 Å), a 2-μm Zn filter (12–16 Å), and a 2-μm Co filter (16–20 Å). The fourth channel used an aluminized mylar filter to sample most (8–20 Å) of the spectrum. Prior to all measurements, we performed a cross-calibration of the individual PCD sensitivities. We did this by recording the signals from each detector using 2-μm Zn filters on each and with all detectors simultaneously illuminated by x rays from an Fe or type 302 stainless steel (SS302) laser-produced plasma. We took several data points for each of three rearrangements of the individual Zn filters so that we could eliminate effects due to variability in the filter transmission. We found variation in detector response among the four devices consistent with a ±20% spread in sensitivity. The extracted filter transmissions were consistent with a 10–15% variability from one piece to the next. Based on these uncertainties alone, the absolute uncertainty in yield for these measurements is around ±25%. Relative uncertainties in comparing different target materials or laser parameters are much better, around 10%, determined primarily by shot-to-shot variations.

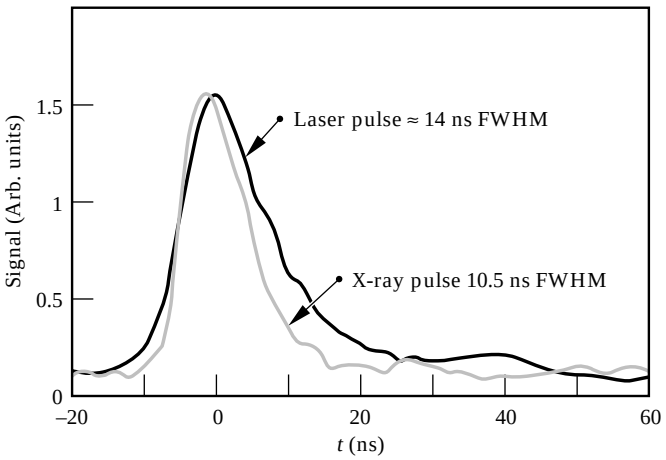

FIGURE 2. Sample oscilloscope traces of the laser pulse measured with a photodiode and an x-ray pulse measured with a photoconductive diamond (PCD) detector. Vertical scales and temporal offsets for both pulses are arbitrary, and were adjusted for comparison. (10-06-0595-1101pb01)

To determine the absolute x-ray yield, we integrated the recorded oscilloscope signals to produce a value proportional to the total x-ray fluence striking the detector. We then converted this raw data value to an absolute measure of the x-ray fluence by factoring in corrections for detector sensitivity, solid angle, filter transmission, and the emission spectrum. Simultaneous measurement of the spectrum is crucial for an accurate determination of the fractional weight of the spectrum viewed by each channel. We determined x-ray yields by multiplying each detector signal by a factor inversely proportional to the known filter response multiplied by the measured spectrum at each incident energy. We then obtained the resulting conversion efficiency from an average of the contributions measured from each channel and the known input laser energy.

The CCD detector on the spectrometer also provided an accurate method of assessing relative x-ray yields (from one target to the next, or for changes in other parameters, such as laser energy). This provided us with a cross-check against the yields inferred on the basis of the PCD measurements. We found good agreement between the relative yields determined from integrating the spectrum recorded on the CCD and the signals measured with the PCD array.

Pinhole Camera

We monitored plasma source size with an x-ray pinhole camera coupled to a video CCD and a computer-controlled readout. We placed the pinhole about 3 cm from the target and operated at a magnification of 2–3. Because it was filtered with 18-μm Al foil, the x-ray spectrum was sensitive mostly to the 8–12-Å portion of the emitted spectrum.

Methods and Results

This section provides specific details about methods and results for the experiment. We divide the section into four subsections: focus optimization, yield variation with pulse energy, x-ray spectra, and angular distribution.

Focus Optimization

For each target type and laser wavelength investigated, we optimized and measured the x-ray yield with a standard procedure consisting of two parts. First, we did a focal scan consisting of a series of shots examining yield as a function of axial lens position at maximum laser energy (20 J at 1.053 μm and 12 J at 0.527 μm). From this procedure, we identified the lens position corresponding to maximum yield as determined by the PCD measurements. Second, with the lens fixed at the maximum yield position, we systematically reduced the laser energy (described in the next section).

Figure 3 shows an example of the variation of x-ray yield with lens position for Cu and type SS302 irradiated with 1.053-µm laser light. We found in general that the x-ray yield reached a broad maximum within ±1 mm of the lens focus. The position of optimum conversion was largely independent of the target material, varying by an amount of approximately ±0.5 mm for different targets.

Figure 4(a) shows pinhole photographs of the x-ray source region throughout the focal scans for 1.053-µm irradiation. The double-lobed structure apparent at lens positions of 14 and 15 mm originates from the intensity distribution in the square beam as it approaches the focus. Similar lobed structures were also evident in the 0.527-µm laser-produced plasmas. Analyzing these images, we assume that the size of the x-ray emitting region correlates with the spatial extent of the laser intensity distribution illuminating the plasma. Figure 4(b) shows the variation of x-ray source size measured in these focal scans. The emitting region of the plasma was considerably larger than the beam diameter close to best focus since under no conditions did we observe an x-ray source region smaller than about 150 µm in diameter, a size 3–5 times larger than the beam diameter expected at best focus for the 1.5× diffraction limited beam. We took the lens position corresponding to best focus to be the point where the observed source diameter reached a minimum. The geometrical extent of the focal cone for the *f*/13 focus is also displayed in these figures for comparison with the data.

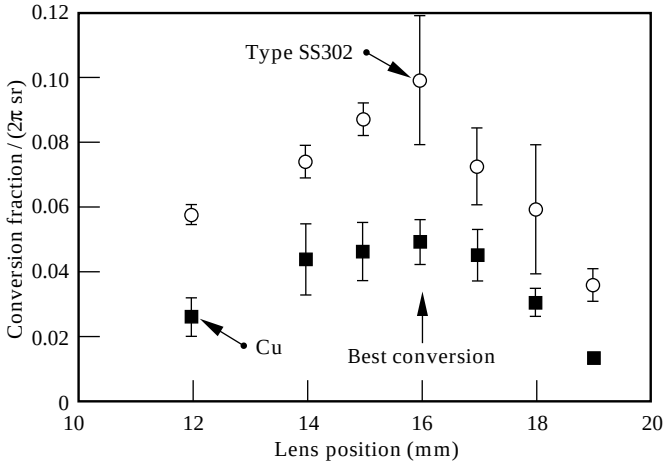

FIGURE 3. Variation of x-ray yield with focusing lens position for 1.053-µm laser light; we used this procedure to optimize the yield for a given target type. (10-06-0595-1102pb01)

The most important information from these sequences is an assessment of the size of the x-ray emitting region in the source and an approximate idea of the laser intensity illuminating the plasma at these optimum positions. At the lens position corresponding to optimum x-ray yield, the diameter of the source region evident from the pinhole images was around 280 µm for 1.053-µm laser light and 240 µm for 0.527-µm light. It is also evident that the focal cone of the *f*/13 focus is smaller than the plasmas at most positions where significant x-ray emission was observed, and that the lens position corresponding to best yield does not correspond to the position of best focus, although it was much closer to best focus for 0.527-µm light than for 1.053-µm light. (X-ray yield on the converging side of the 1.053-µm focused beam should be similar to the diverging side; for all measurements reported here the beam was focused on target with a diverging focus.) Average

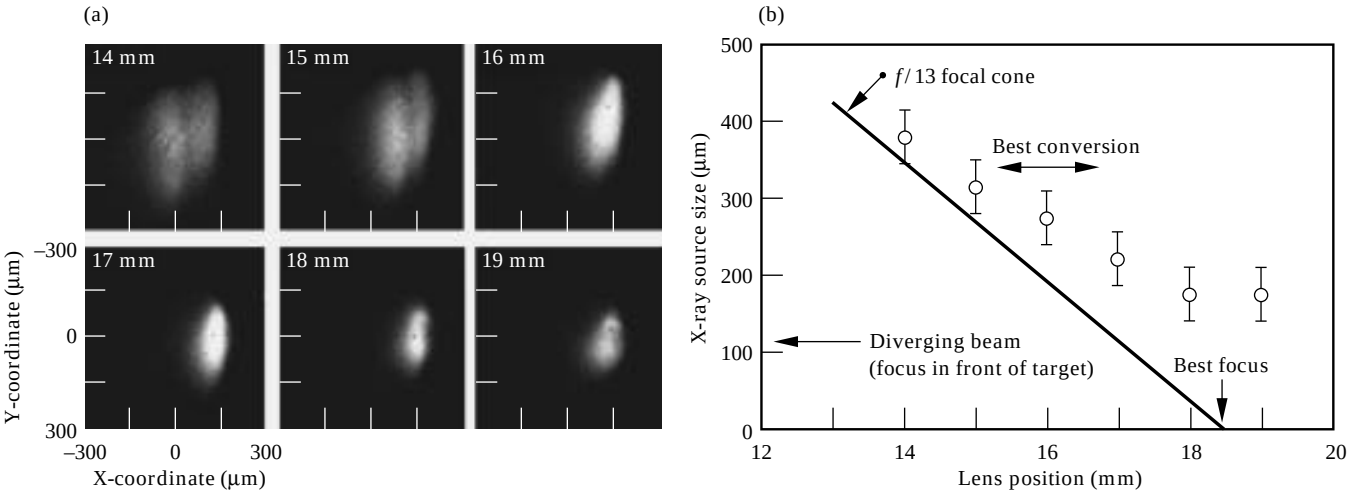

FIGURE 4. Variation of x-ray emitting plasma volume with focusing lens position for 1.053-µm laser light irradiating a solid Fe target. The origin of the lens position scale is arbitrary. (a) A sequence of pinhole photographs of the plasma x-ray emission taken at various lens positions (indicated on the individual frames). (b) Variation of plasma size with lens position measured from the pinhole photographs. Also shown for comparison is the beam size assuming a geometric *f*/13 focal cone with best focus assumed to occur at the lens position producing the smallest plasma volume. (10-06-0595-1103pb01)

beam intensities illuminating the plasma at these lens positions can be estimated from the geometrical extent of the focal cone and the distance of the optimum lens position from best focus. For 1.053-μm light, the beam diameter at optimum focus was ~190 μm, to produce a beam intensity $\sim 5 \times 10^{12}$ W / cm^2. For 0.527-μm light, the beam diameter was approximately 100 μm, a factor of two smaller than for the optimum 1.053-μm situation, producing intensities $\sim 1.2 \times 10^{13}$ W / cm^2.

Yield Variation with Pulse Energy

After we determined the optimum focus position, we fixed the lens at its optimum position and measured x-ray yields while the laser energy was varied throughout the available range below the maximum setting. We easily adjusted laser energy by varying a waveplate within the preamplifier chain to control the pulse energy prior to the final amplifier passes. Both the temporal pulse shape and spatial beam parameters (focus position) were unaffected by this adjustment.

An important characteristic of all of the measurements from planar targets measured in this research was an increasing x-ray yield with pulse energy. For all materials, the conversion increased monotonically from near zero at low pulse energies and increased to a saturation value before leveling off. Figure 5 shows an example of this dependence for (a) type SS302 and (b) Cu. Within the energy range available there was no evidence of a regime where conversion fraction decreased with increasing pulse energy. The saturation value varied with the target material and the laser wavelength. With type SS302 (median emission wavelength at 15 Å), the laser energy at saturation is clearly lower than for Cu (median emission wavelength at 11.5 Å). In the case of Cu, it is not clear that the dependence of x-ray yield with energy has reached a final saturation level at the maximum laser pulse energies available in these experiments, although saturation appears to be ~5–10 J for type SS302. Correlated with the pulse energy dependence of yield was a clear shift in the x-ray spectrum for any given target to shorter wavelengths (harder photons) with increasing pulse energy. We expected this due to the fact that increasing pulse energies produce higher intensities and drive hotter plasmas.

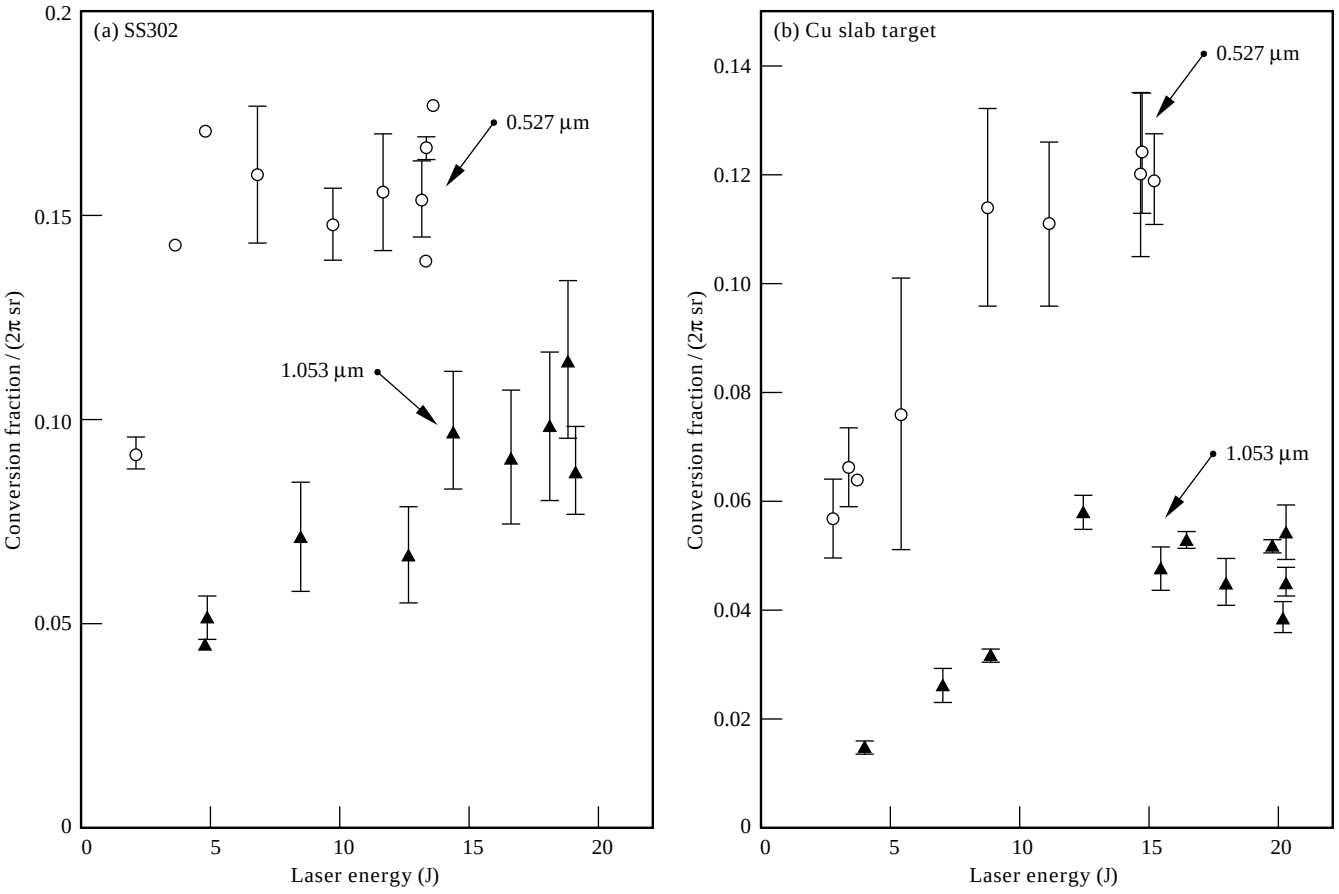

FIGURE 5. Pulse energy dependence of x-ray yield for two target materials and both drive wavelengths. Target materials are (a) type SS302 and (b) Cu. (10-06-0595-1104pb01)

X-Ray Spectra

Figure 6 shows a catalogue of spectra for all of the materials tested using 0.527-μm laser light. Also identified on the spectra are integral curves depicting the integrated conversion fraction through the short to long range of emission wavelengths. We observed a similar set of spectra using 1.053-μm light, with the main difference being a shift in the distribution of emission to longer wavelengths within the characteristic spectrum of each material. For the materials selected, Fig. 7 summarizes the x-ray wavelength range (10–15 Å).

All of the Xe spectra exhibit a bilobed distribution of emission with a main component emitting at wavelengths from 10–15 Å, and a second component from 17–20 Å. We also included this latter component, accounting for about 20–30% of the emitted energy, in our yield determination, although the component is of little use for lithography applications. Excluding this component (i.e., excluding wavelengths >16 Å), the Xe conversion measured with 1.053-light is less than 10%, but still comparable to the type SS302 conversion. With 0.527-μm light the Xe spectrum becomes harder, shifting to shorter wavelengths, and the total conversion improves to around 12%.

The conversion efficiency measured with type SS302 is significantly higher than with pure Fe. We can attribute this largely to the addition of significantly more spectral lines with contributions from Cr, Mn, Ni, etc., present in the stainless steel alloy. Figure 6(b) demonstrates this, showing the dense spectrum of stainless steel as compared with the pure Fe spectrum in Figure 6(c). We discuss this improved conversion efficiency later in the article.

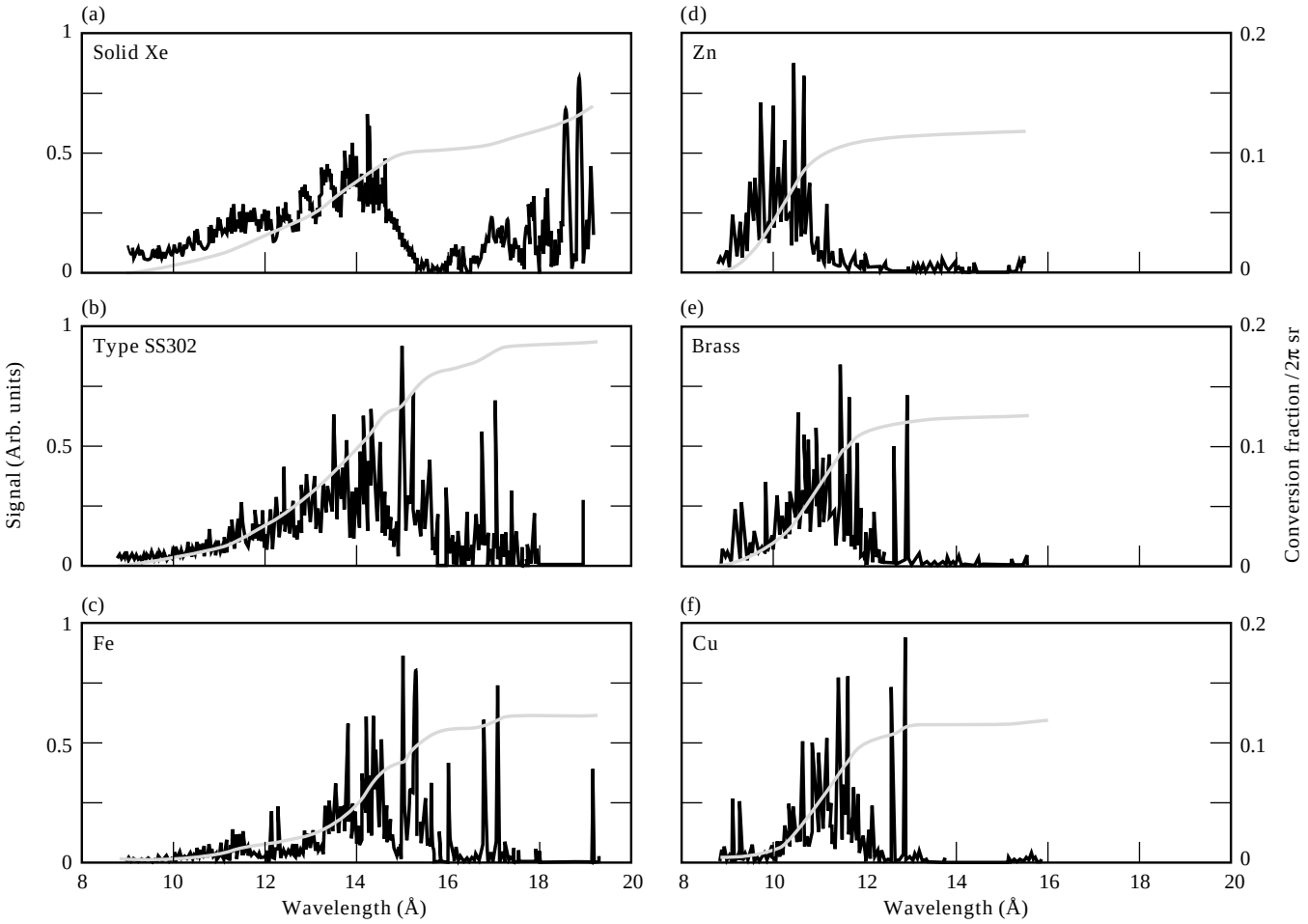

FIGURE 6. X-ray spectra measured for all solid targets using 0.527-μm laser light. Spectral intensity is displayed on the arbitrary left hand scale; the wavelength-integrated x-ray yield for each material can be measured against the right hand scale. Conversion fraction indicates the ratio of x-ray energy to incident laser energy. Target materials are (a) solid Xe, (b) type SS302, (c) Fe, (d) Zn, (e) brass, and (f) Cu.
(10-06-0595-1105pb01)

Angular Distribution

For planar targets, we also measured the angular distribution of x-ray yield. We recorded all yield measurements with the PCD array at target normal, where the yield is expected to reach a maximum. For historical reasons, and to ease comparison with other work, we report the x-ray yield as the conversion fraction into 2π sr as if the angular distribution were isotropic and equal to the angular fluence measured at target normal. In general, the angular fluence varies relative to target normal and depends on target material, laser wavelength, laser pulse duration, and possibly other factors. The yield is generally reduced away from target normal and can be fitted with a $\cos^{\alpha}\theta$ distribution, where $\alpha \leq 1$, and the total conversion into 2π sr is less than the fraction reported in this work. There may be reasons to place the lithography exposure system at a location other than target normal; for example, to mitigate against debris, which is also maximized at target normal. Thus an assessment of the angular distribution is important to ascertain any reduction in x-ray yield at other angles.

We did the angular distribution measurements for Fe and type SS302 targets at the optimized conditions for both wavelengths. We fitted all PCD detectors with 2-µm Zn filters, which transmit the main component of the Fe spectrum. We arranged the detectors in four angular positions in the plane of the laser beam spanning angles from 18–75° from the target normal. We took several sets of shots for each measurement, for which the Zn filters were rotated through the detectors, to eliminate effects due to variations in the filter transmissivities. We discuss results from these measurements in the next section.

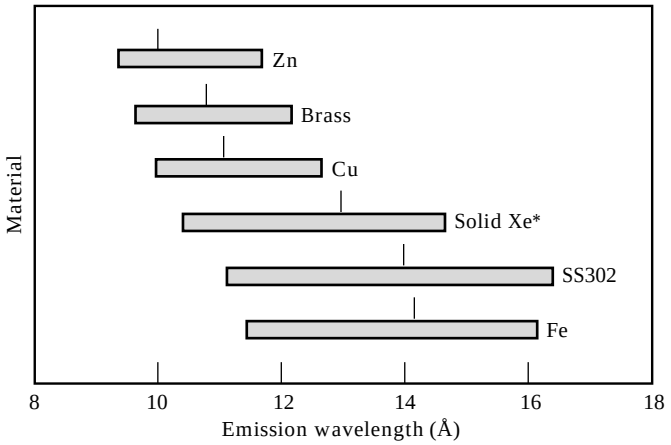

FIGURE 7. Emission wavelengths determined from the spectra measured for all the solid elements using 0.527 µm laser irradiation. The bar end points indicate wavelengths spanning 10 to 90% of the wavelength-integrated emission (i.e., containing 80% of the emission). The points within the bars indicate the median emission wavelengths (50% point on the integral curve) for each material. *In the special case of Xe, this evaluation was restricted to wavelengths less than 16 Å, which eliminates the long-wavelength emission component (~18 Å) from the weighting process. (10-06-0595-1108pb01)

Discussion

There are four main areas of discussion for this experiment: x-ray yields and spectra, pulse energy dependence, laser-drive wavelength dependence, and angular distribution.

X-Ray Yields and Spectra

Figure 8 summarizes x-ray yields from all of the solid targets, and compares the optimized yield for each material at both wavelengths. We obtained high x-ray yields using the longer wavelength emitters (~14 Å) with 1.053-µm laser-drive wavelength, the best examples of these being type SS302 and cryogenic Xe. Conversion efficiency of these targets was approximately 10% / (2π sr) at the target normal. Conversion for shorter wavelength emitters using 1.053-µm was significantly less, dropping to <4% / (2π sr) for Zn targets emitting at around 10.5 Å. We observed a significant improvement in x-ray conversion with 0.527-µm light, where conversion efficiencies for all targets was ~12% / (2π sr) or better. For the range of shorter-wavelength emitters, including Cu, brass, and Zn, this represents a factor of 3–4 improvement in the yield measured at target normal. Since the energy conversion efficiency for doubling the laser-light frequency is expected to be around 80%,[21] this result indicates that operation at 0.527 µm will provide a substantial improvement in conversion of energy from the fundamental laser wavelength to x rays in the 10–12-Å band using a frequency-doubled laser.

Solid Xe offers the attractive possibility of building a reduced-debris source. The Xe spectrum contains two main components, with a longer-wavelength portion occupying the 17–20 Å. For lithography, the 75–80% energy portion of the spectrum emitted in the 10–14 Å band is the most useful part. With 0.527-µm laser irradiation, this portion of the spectrum is significantly

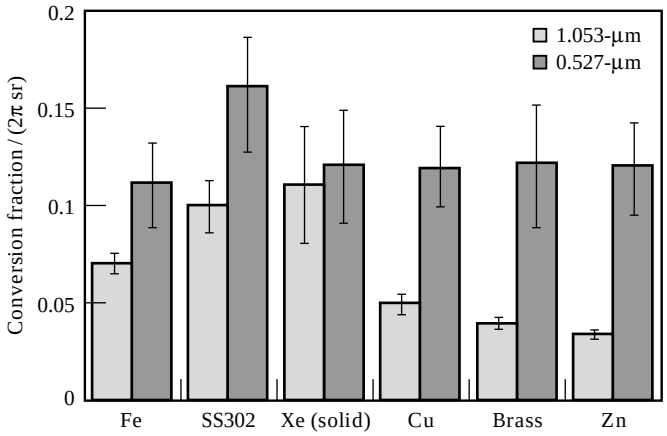

FIGURE 8. Optimized x-ray yields measured for all solid targets and both drive wavelengths. (10-06-0595-1107pb01)

harder than with 1.053-µm irradiation. Solid Xe provides x-ray yields comparable to, or better than, other solid targets at both drive wavelengths investigated. In the form of cryogenic pellets, frozen Xe offers the potential for producing a reduced-debris source with yields comparable to other solid target yields.

We attained the best yields with type SS302 targets. The improvement in conversion efficiency compared with pure Fe targets is apparent with 1.053-µm laser light, and becomes quite dramatic with 0.527-µm light, where the optimum conversion efficiency exceeds 16% for type SS302. Stainless steel is an alloy comprised mainly of several transition metals with atomic numbers from Z = 24 through Z = 28 (the chemical composition of type 302 is approximately 70% Fe, 18% Cr, 9% Ni, and 2% Mn). These elements emit kilovolt radiation efficiently in the plasmas produced by the laser. The increased yield from the alloy occurs because the strongly emitting lines characteristic of each element are optically thick, or nearly so in these high-density plasmas produced with solid targets; thus, the reduced concentration of Fe found in stainless steel as compared with pure Fe targets does not lead to a noticeable reduction in the intensity of the characteristic Fe spectral components, while the other alloyed elements in stainless steel provide emission features that fill the gaps in the spectrum. This result indicates the possibility for improving x-ray yields by designing mixtures of elements that emit in the desired wavelength band. These will produce high yields by filling in the spectrum with more lines. The high yields of Xe are produced for a similar reason, namely that the much more complicated electronic structure of the Xe M-shell provides many more emission lines to fill in the spectral band than the simpler L-shell emitters.

Pulse Energy Dependence

The pulse energy dependence of the observed x-ray yield is most easily understood in light of previous 0.5-ns pulse duration work by Chaker et al.[16], in which the conversion efficiency into kilovolt x rays from Cu targets was observed to drop abruptly below intensities of $\sim 5 \times 10^{12}$ W/cm^2 for 1.06-µm light. Optimum conversion efficiencies for Cu measured in this work are comparable to the values reported by Chaker et al. As noted, our procedure for optimizing the conversion by scanning the focus automatically places the irradiance near this saturation intensity and not necessarily at the best focus. Consequently, the measurements at decreasing pulse energy will produce lower than optimum intensities, and therefore produce lower x-ray yields. An implication of this interpretation is that it may be possible to attain high yields at lower pulse energies using a faster focusing lens (e.g., $f/4$ instead of $f/13$) that achieves $\sim 10^{13}$ W/cm^2 within the beam focus. However, we stress that achieving 10^{13} W/cm^2 is necessary but may not be sufficient to achieve high yields (with long pulses)—this possibility needs to be explored experimentally. In our research, we made no attempts to exploit this method of obtaining high conversion efficiency at lower pulse energies.

Laser-Drive Wavelength Dependence

As a general rule, the conversion fraction (laser energy to x-ray energy) into 2π sr is higher at 0.527 µm than at 1.053 µm. The phenomenon is most accentuated for the short wavelength (10–12-Å) emitters (Cu, Zn, and brass), where the conversion fraction improves by a factor of 3–4 times over the 1.053-µm result. This dramatic improvement in conversion for the shorter-wavelength emitters using frequency-doubled laser light more than compensates for losses introduced by converting the fundamental to the second harmonic, and provides a means to obtain high x-ray yields at a range of desired wavelengths from 10.5 Å (Zn) to 15 Å (SS302) with a single laser driver.

As increasing pulse energy causes spectral shifts, changing the drive wavelength from 1.053 to 0.527 µm clearly caused the spectra of the various target types to shift to shorter wavelengths. This spectral dependence is consistent with (1) the improved coupling of the laser light into plasma heating at higher densities and (2) the improved conversion. Figure 9 shows an example of this spectral shift for solid Xe targets. We observed similar laser-drive-wavelength-dependent spectral shifts for the other materials investigated.

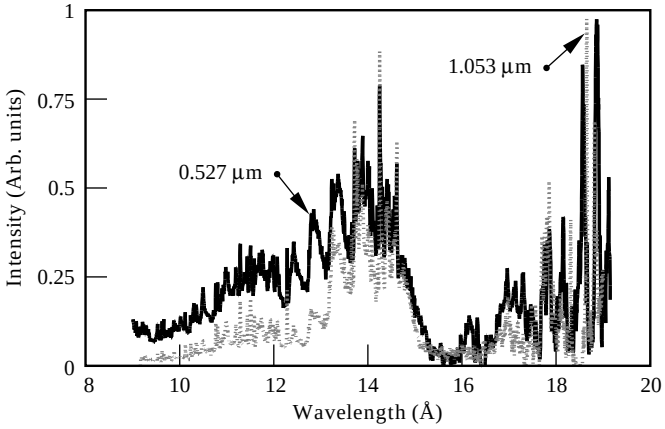

FIGURE 9. Comparison of x-ray spectra from solid Xe measured from plasmas produced with 1.053-µm (dashed line) and 0.527-µm (solid line) laser light. (20-07-0695-1659pb01)

Angular Distribution

Figure 10 shows the angular distributions measured for both drive wavelengths irradiating Fe or type SS302 targets. Fits to a $\cos^{\alpha}\theta$ distribution yielded $\alpha \approx 0.2$ for 1.053-µm irradiation and $\alpha \approx 0.6$ for 0.53-µm irradiation. Neither of these angular distributions is Lambertian ($\alpha = 1$). At 1.053 µm, the emission is very close to being isotropic, such that at angles of 60–70° from the target normal, the observed yield remains at 80% or more of the peak yield at target normal. At 0.53 µm the emission is closer to Lambertian, with the yield reduced to half of the peak at angles of >65° off target normal. The difference in angular distribution reflects the difference in laser light coupling between the two wavelengths. The shorter wavelength couples much more efficiently into higher density plasma layers, which are optically thick and closer to the target plane, thus producing a physical situation that is close to that of a planar, optically thick Lambertian surface emitter.

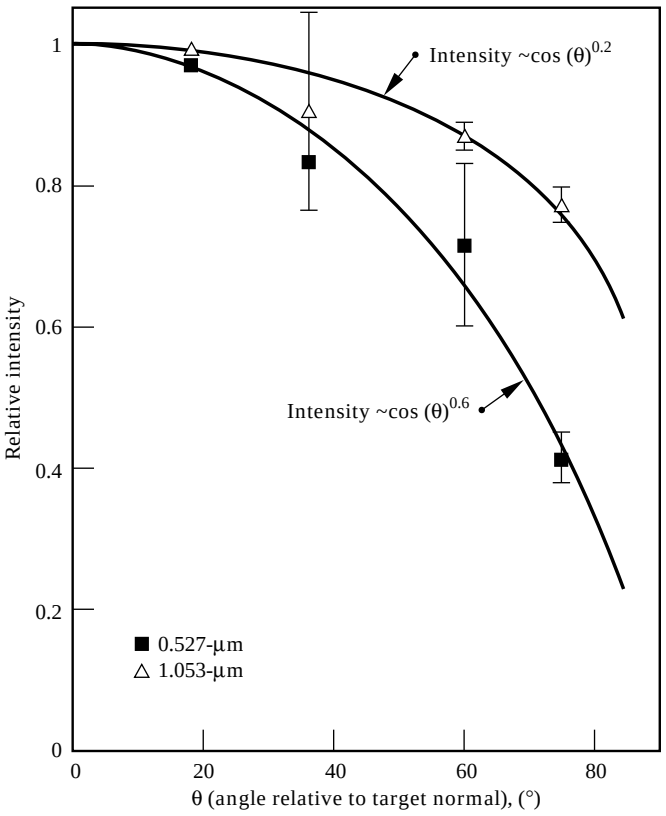

FIGURE 10. Angular distribution of x-ray emission relative to target normal measured for 14-Å emitters Fe or type SS302 at both drive wavelengths. (10-06-0595-1106pb01)

Conclusions

The intended operating x-ray wavelength of a proximity lithography system will be determined by a number of considerations beyond the scope of the present study. For most situations, x-ray wavelengths spanning the range from 10–15 Å may be used. The materials selected in this study embrace this wavelength region. These results demonstrate a significant degree of flexibility in delivering x-ray energy within a desired wavelength band using a laser-produced plasma.

X-ray conversion efficiency from all targets increased with increasing laser pulse energy from small values at low pulse energies (<5 J). A minimum pulse energy of ~5–10 J was necessary to approach the yields close to the optimum. Above ~10 J, the yield vs pulse energy curve begins to saturate. This behavior is consistent with the observed saturation of conversion with laser intensity observed by Chaker et al.[16] using 0.5-ns pulses, thus indicating that the 10-ns plasma behaves similarly in this pulse energy range. At optimum conditions, the average intensity illuminating the plasma was approximately 5×10^{12} W/cm^2 for 1.053-µm light, and 1×10^{13} W/cm^2 for 0.527-µm light. For both wavelengths the source diameter at optimum conversion was ~250–300 µm.

The x-ray conversion efficiencies produced with the long-pulse laser driver used in these experiments matched efficiencies measured previously with shorter (nanosecond-duration) pulses. The duration of the x-ray pulse matched the duration of the laser pulse, indicating that, at least in the 12–14-ns range, the long pulse duration does not degrade the conversion efficiency. A frequency-doubled Nd:glass laser driver can be used to produce a source with median emission wavelength anywhere from 10.5 to 15 Å at x-ray yields that meet the needs of a proximity lithography production system.

Acknowledgments

We acknowledge technical support from Jim Wintemute for operating the laser, as well as Jim Cox and Ken Haney for fabrication and assembly of the target facility, and Joe Smith for filter calibrations. This work was supported by a contract from the U.S. Department of Defense Advanced Research Projects Agency.

Notes and References

1. J. Warlaumont, *J. Vac. Sci. Technol. B7*, 1634 (1989).
2. G. Zwicker, W. Windbracke, H. Bernt, D. Friedrich, H.-L. Huber, et al., *J. Vac. Sci. Technol. B7*, 1642–1647 (1989).
3. K. M. Gilbert, J. P. Anthes, M. A. Gusinow, M. A. Palmer, et al., *J. Appl. Phys.* 51, 1449–1451 (1980).
4. B. Yaakobi, P. Bourke, Y. Conturie, J. Delettrez, J. M. Forsyth, et al., *Opt. Commun.* 38, 196–200 (1981).
5. H. Nishimura, F. Matsuoka, M. Yagi, K. Yamada, et al., *Phys. Fluids* 26, 1688–1692 (1983).
6. D. L. Matthews, E. M. Campbell, N. M. Ceglio, G. Hermes, R. Kauffman, et al., *J. Appl. Phys.* 54, 4260–4268 (1983).
7. W. C. Mead, E. M. Campbell, K. G. Estabrook, R. E. Turner, W. L. Kruer, et al., *Phys. Fluids* 26, 2316–2331 (1983).
8. P. Alaterre, H. Pépin, R. Fabbro, and B. Faral, *Phys. Rev. A* 34, 4184–4194 (1986).
9. T. Mochizuki, T. Yabe, K. Okada, M. Hamada, N. Ikeda, S. Kiyokawa, and C. Yamanaka, *Phys. Rev. A* 33, 525–539 (1986).
10. R. Popil, P. D. Gupta, R. Fedosejevs, and A. A. Offenberger, *Phys. Rev. A* 35, 3874–3882 (1987).
11. K. Eidmann and W. Schwanda, *Laser and Particle Beams* 9, 551–562 (1991).
12. J. N. Broughton and R. Fedosejevs, *Appl. Phys. Lett.* 60, 1818–1821 (1992).
13. D. J. Nagel, M. C. Peckerar, R. R. Whitlock, J. R. Greig, and R. E. Pechacek, *Electron. Lett.* 14, 781–782 (1978).
14. B. Yaakobi, H. Kim, J. M. Soures, H. W. Deckman, and J. Dunsmuir, *Appl. Phys. Lett.* 43, 686–688 (1983).
15. H. Pépin, P. Alaterre, M. Chaker, R. Fabbro, B. Faral, et al., *J. Vac. Sci. Technol. B* 5, 27–32 (1987).
16. M. Chaker, H. Pépin, V. Bareau, B. Lafontaine, I. Toubhans, et al., *J. Appl. Phys.* 63, 892–899 (1988).
17. G. M. Davis, M. C. Gower, F. O'Neill, and I. C. E. Turcu, *Appl. Phys. Lett.* 53, 1583–1585 (1988).
18. M. Chaker, B. L. Fontaine, C. Y. Côté, J. C. Kieffer, H. Pépin, et al., *J. Vac. Sci. Technol. B* 10, 3239–3242 (1992).
19. M. Chaker, J. F. Pelletier, and J. C. Kieffer, in *Materials Aspects of X-Ray Lithography*, G. K. Celler and J. R. Maldonado, Eds. (Materials Research Society, San Francisco, CA, USA, 1993) pp. 151–167.
20. R. Kodama, T. Mochizuki, K. A. Tanaka, and C. Yamanaka, *Appl. Phys. Lett.* 50, 720–722 (1987).
21. C. B. Dane, L. E. Zapata, W. A. Neuman, M. A. Norton, and L. A. Hackel, *IEEE J. Quantum Electron.* 31, 148–163 (1995).
22. C. B. Dane, W. A. Neuman, and L. A. Hackel, *Opt. Lett.* 17, 1271–1273 (1992).
23. Princeton Instruments, Inc., 3660 Quakerbridge Rd., Trenton, NJ, 08619 USA.
24. B. L. Henke, P. Lee, T. J. Tanaka, R. L. Shimabukuro, and B. K. Fujikawa, *At. Data Nucl. Data Tables* 27, 1–144 (1982).
25. D. R. Kania, L. Pan, H. Korblum, P. Bell, et al., *Rev. Sci. Instrum.* 61, 2765–2767 (1990).
26. D. R. Kania, H. Kornblum, B. A. Hammel, J. Seely, C. Brown, et al., *Phys. Rev. A* 46, 7853–7868 (1992).
27. D. R. Kania, L. S. Pan, P. Bell, O. L. Landen, H. Kornblum, et al., *J. Appl. Phys.* 68, 124–130 (1990).